Quantum dot/antibody conjugates for in vivo cytometric imaging in mice

Hee-Sun Han[a], Elisabeth Niemeyer[b], Yuhui Huang[b], Walid S. Kamoun[b], John D. Martin[b,c], Jayeeta Bhaumik[b], Yunching Chen[b], Sylvie Roberge[b], Jian Cui[a], Margaret R. Martin[b], Dai Fukumura[b], Rakesh K. Jain[b,1], Moungi G. Bawendi[b,1], and Dan G. Duda[b]

Departments of [a]Chemistry and [c]Chemical Engineering, Massachusetts Institute of Technology, Cambridge, MA 02139; and [b]Edwin L. Steele Laboratory, Massachusetts General Hospital and Harvard Medical School, Boston, MA 02114

Contributed by Moungi G. Bawendi, November 12, 2014 (sent for review June 10, 2014)

Multiplexed, phenotypic, intravital cytometric imaging requires novel fluorophore conjugates that have an appropriate size for long circulation and diffusion and show virtually no nonspecific binding to cells/serum while binding to cells of interest with high specificity. In addition, these conjugates must be stable and maintain a high quantum yield in the in vivo environments. Here, we show that this can be achieved using compact (~15 nm in hydrodynamic diameter) and biocompatible quantum dot (QD) -Ab conjugates. We developed these conjugates by coupling whole mAbs to QDs coated with norbornene-displaying polyimidazole ligands using tetrazine–norbornene cycloaddition. Our QD immunoconstructs were used for in vivo single-cell labeling in bone marrow. The intravital imaging studies using a chronic calvarial bone window showed that our QD-Ab conjugates diffuse into the entire bone marrow and efficiently label single cells belonging to rare populations of hematopoietic stem and progenitor cells ($Sca1^+c\text{-}Kit^+$ cells). This in vivo cytometric technique may be useful in a wide range of structural and functional imaging to study the interactions between cells and between a cell and its environment in intact and diseased tissues.

quantum dots | in vivo imaging | single cell imaging | in vivo cytometry | multiphoton microscopy

Studying migration of individual endogenous cells and their interactions with the surrounding microenvironment in vivo would greatly help expand our knowledge on how cells behave in their complex native biological network. However, single-cell imaging of a rare population in vivo places highly stringent constraints on targeting fluorophores. First, identifying specific cell populations among various types of cells expressing overlapping surface markers demands simultaneous labeling of multiple markers, and therefore requires fluorophores with narrow emission features. Second, the size of targeting fluorophore conjugates needs to be optimized to simultaneously achieve both long blood circulation times and high diffusion in dense in vivo environments. Third, because only a small fraction of systemically administered fluorophores is delivered to the targeting sites, resulting in low signal, targeting fluorophore conjugates must emit bright signals and exhibit minimal nonspecific binding to serum proteins and cells. Fourth, targeting fluorophore conjugate samples must be free of unbound targeting molecules, because unbound targeting molecules can block target sites and yield decreased signal.

Because of the lack of such a technology, direct labeling of single cells from an endogenous rare cell population in live and nonmanipulated animal models has not been possible. Instead, researchers have used (*i*) immunohistochemistry (1), (*ii*) ex vivo (2) or intravital imaging (3) of injected target cells, which are fluorescently labeled ex vivo, or (*iii*) ex vivo (4) or intravital imaging (5, 6) of target cells that are genetically modified to express fluorescent markers. However, none of these methods reproduce the native microenvironment of target cells. Tissue immunohistochemistry and ex vivo imaging only provide a snapshot image of a perturbed state. Intravital imaging allows for real-time imaging but requires either genetically engineered mouse models to induce endogenous expression of fluorescence proteins in cells or irradiation of mice for marrow depletion and repopulation with systemically infused cells.

Quantum dots (QDs) possess unique optical properties that are ideal for in vivo imaging in live animals. Specifically, QDs have a tunable band gap ranging from the visible to the IR, high quantum yields (QYs), narrow and symmetric emission features, broad absorption above the band gap, large multiphoton absorption cross-sections, and high photostability (7–10). These properties make QDs amenable to optical multiplexing for simultaneous study of various targets, long-term tracking, and deep-tissue imaging using multiphoton microscopy. Despite these exciting capabilities, most imaging studies using QDs have involved either in vitro targeting or ensemble measurements of QD signals over large volumes of tissue in vivo (11–15). This restriction is caused by a lack of technology for synthesizing QD conjugates that are optimal for single-cell imaging in vivo.

Here, we report the development of QD-Ab conjugates that satisfy all of the constraints described above. Moreover, we used these QD-Ab conjugates for in vivo cytometry of endogenous bone marrow cells (BMCs) in their unperturbed microenvironment. Our technique provides opportunities to study the movements of single cells and the interactions between cells and between a cell and its environment in their native states.

Synthesis and Characterization of QD-norbornene–tetrazine-Ab

We previously developed polyimidazole ligands (PILs) incorporating norbornene (NBPILs) for QDs (16). PILs (random copolymers

Significance

One of the key questions in biology is understanding how cells move, interact, and evolve in living organisms. Tremendous efforts have been made to answer these questions in vitro, which have yielded a molecular-level understanding of cellular events. However, an increasing number of studies indicate that cellular activities need to be understood in the context of their natural environments. Single-cell labeling methods in use currently involve immunohistochemistry, genetic manipulation, or irradiation of mice, none of which reflect the native microenvironments. Here, we report quantum dot immunoconstructs that can be used for intravital imaging of single cells in unmanipulated mice and multiplexed in vivo cytometric analysis of rare cell populations.

Author contributions: H.-S.H., D.F., R.K.J., M.G.B., and D.G.D. designed research; H.-S.H., E.N., Y.H., W.S.K., J.D.M., J.B., Y.C., S.R., and J.C. performed research; H.-S.H. contributed new reagents/analytic tools; H.-S.H., Y.H., W.S.K., J.D.M., and M.R.M. analyzed data; and H.-S.H., M.G.B., and D.G.D. wrote the paper.

The authors declare no conflict of interest.

[1]To whom correspondence may be addressed. Email: jain@steele.mgh.harvard.edu or mgb@mit.edu.

This article contains supporting information online at www.pnas.org/lookup/suppl/doi:10.1073/pnas.1421632111/-/DCSupplemental.

incorporating imidazole and PEG) effectively passivate the QD surface to achieve a high QY in aqueous solution (80–90%). PIL-coated QDs show greatly enhanced stability in buffers and blood sera, because the multidentate imidazole motifs of PILs are chemically stable and exhibit a high affinity toward the Cd- and Zn-rich QD surfaces (17). Norbornene, an uncharged functional group, allows incorporation of a high number of derivable functional groups while maintaining an overall neutral charge. In contrast, conventional QDs displaying amine or carboxyl groups suffer from nonspecific binding to cells and biomolecules because of their surface charge. Implementing the advantages described above, we synthesized QD conjugates [QD-norbornene–tetrazine-Ab conjugates (QD^{NB}-^{Tz}Ab)] by coupling NBPIL-coated QDs with tetrazine-modified Abs. In detail, QD^{NB}-^{Tz}Abs were synthesized by exchanging the native ligand of QDs with NBPILs and coupling whole antibodies to QDs using tetrazine–norbornene cycloaddition as shown in Fig. 1*A*. Tetrazine-modified antibodies were prepared by reacting a tetrazine derivative with the lysine groups of antibodies followed by immediate conjugation to the QD^{NB} by mixing the two components at room temperature. In this study, we synthesized QD^{NB}-^{Tz}Ab conjugates with diverse combinations of QDs [CdSe/CdZnS (QD_{612}), CdSe/CdS (QD_{570}), and InAs/CdZnS (QD_{800})] and mAbs (anti-mouse CD31, CD45, c-Kit, and Sca-1 antibodies or isotype-matched IgG).

Purification of free antibodies from QD^{NB}-^{Tz}Ab was essential to achieve single-cell labeling in vivo. Without purification, single-cell labeling results were inconsistent, and the labeling signal intensities were extremely low. Inconsistencies and low signals were caused by free antibodies left in the conjugate solution that bind to targeting antigens on the cell surface and block the binding of QD probes. The presence of free antibodies can drastically interfere with the binding of QD probes in vivo due to the following reasons. First, systemically injected QDs are delivered to the target cells by extravasation from vessels and diffusion throughout the interstitial space, and therefore, the effective concentration of the probes around the target cells is low. Second, the hydrodynamic diameter (HD) of free antibodies (~12 nm) is slightly smaller than that of QD conjugates (15–17 nm), yielding faster extravasation and diffusion. A previous method to conjugate EGF, a 6,045-Da protein with an HD of 2.7 nm, to QDs (16) utilizes dialysis filters to purify unconjugated proteins. However, an Ab (a 150-kDa protein with an HD of 12 nm) has a similar size and charge as a QD, and therefore, it is difficult to separate the two using commonly used size- or charge-based purification methods. Instead, free antibodies were successfully purified using gradient centrifugation. Separation using this method is based on density, with denser QDs and QD-Ab conjugate moving faster than free antibodies (*SI Appendix*, Fig. S1).

The hydrodynamic size of nanomaterials influences their biological accessibility, local distribution, and clearance in a live animal, and it can affect the motion of the targeted species (12, 13, 18, 19). To achieve sufficient transvascular permeability and interstitial diffusion, QD^{NB}-^{Tz}Ab was made as compact as possible by optimizing the incubation duration of QD^{NB} with ^{Tz}Ab and quenching unreacted tetrazine on the antibodies using 5-norbornene-2,2-dimethanol to prevent additional aggregation. Polyimidazole ligands also contribute to the small HD of our QD conjugates, because they directly bind to the QD surface (coordinating ligands). In contrast, typical commercial water-soluble QDs are prepared by encapsulating hydrophobic QDs with amphiphilic polymers and therefore, display higher HD. Dynamic light scattering measurements show that both QD_{612}^{NB} and QD_{612}^{NB}-^{Tz}Ab were more compact than commercial Qdot 625 and Qdot 625-Ab (Life Technologies) (Fig. 1*B* and Table 1).

Charge has a major effect on the transport behavior of nanoparticles in vivo and in vitro (20). A high surface charge, either positive or negative, tends to trigger nonspecific uptake of the particles by macrophages and results in more accumulation of the particles in the liver than in the targeting region after systemic administration. ζ-Potential measurements indicate that the surfaces of our QD^{NB} and QD^{NB}-^{Tz}Ab conjugates were moderately negative (Fig. 1*C* and *SI Appendix*, Table S2).

Minimizing nonspecific protein adsorption on nanoparticles is critical for single-cell targeting in vivo. Nonspecific protein adsorption on particles not only hinders the application of the particles to specific targeting but also, can trigger unwanted biological responses in vivo. The level of nonspecific interaction of our QD probes with serum proteins was evaluated by incubating QD^{NB} emitting at 612 nm (QD_{612}^{NB}) in FBS at 37 °C for 4 h and monitoring the size change. The sizes of the QDs before and after incubation were measured using fluorescence correlation spectroscopy (*SI Appendix*, Fig. S2 and Table S5) and dynamic light scattering. As shown in Table 1, the HD of QD_{612}^{NB} did not change after incubation in serum, indicating that QD_{612}^{NB} does not absorb serum proteins nonspecifically. In contrast, commercial Qdot 625 (Life Technologies) showed a significant size increase after serum incubation (Table 1).

In Vitro Specificity Study

The targeting specificity of QD^{NB}-^{Tz}Ab was first tested in vitro using flow cytometry (Fig. 2). First, nonspecific binding of the QD^{NB} and the QD^{NB}-^{Tz}Ab on cells was tested by incubating QD_{570}^{NB}, QD_{612}^{NB}, and QD_{570}^{NB}-^{Tz}Ab(IgG) with peripheral blood mononuclear cells (PBMNCs), which were obtained from mice after lysis of RBCs. Ab(IgG) stands for nonspecific control IgG, which should show no binding ability. We did not detect any nonspecific adsorption of the QDs and the QD^{NB}-^{Tz}Ab(IgG) on the PBMNCs

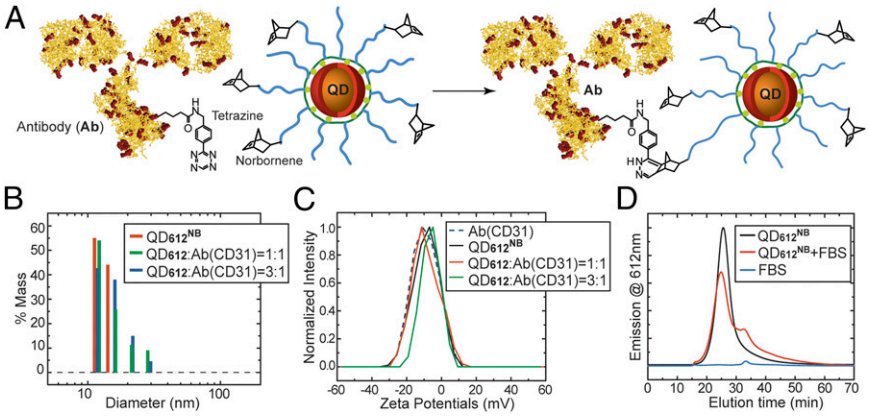

Fig. 1. QD^{NB}-^{Tz}Ab nanoconjugate synthesis and characterization. (*A*) Conjugation of QDs to Abs. Ab (IgG_{2a}) is used to represent the Ab, and Lys residues of Ab(IgG_{2a}) are marked in red. This diagram is not to scale. (*B*) Dynamic light scattering data of the QDs and the QD^{NB}-^{Tz}Ab illustrate that QD^{NB}/Ab conjugation does not yield noticeable aggregates and that the size of QD^{NB}-^{Tz}Ab is compact. (*C*) ζ-Potential measurements of the QDs and the QD^{NB}-^{Tz}Ab show that the surface charge of QD^{NB} and QD^{NB}-^{Tz}Ab is moderately negative. (*D*) Gel filtration chromatography (GFC) traces of QD_{612}^{NB} before and after serum incubation show that there is virtually no nonspecific binding of QD^{NB} to serum proteins.

Table 1. HD of QDs or QD-Ab conjugates measured using dynamic light scattering and fluorescence correlation spectroscopy

QDs or QD conjugates	Inorganic diameter (nm)	Average HD (nm)
QD_{612}^{NB}*	5.8 ± 0.5	12.5 ± 0.2
QD_{612}^{NB} + FBS, 37 °C/4 h†		12.6 ± 0.2
QD_{612}:Ab(CD31) = 1:1*		15.1 ± 0.3
QD_{612}:Ab(CD31) = 3:1*		17.4 ± 0.6
Qdot 625 (Invitrogen)*	9.0 ± 1.0	20.0 ± 0.5
Qdot 625 + FBS, 37 °C/4 h†		33.4 ± 2.6
Qdot 625-Ab(CD31)*		20.5 ± 0.6

*Measured using dynamic light scattering.
†Measured using fluorescence correlation spectroscopy.

(*SI Appendix*, Fig. S8). We then incubated the PBMNCs with $QD_{612}^{NB\text{-}Tz}$Ab(CD45), a leukocyte marker. After incubation, >75% of the PBMNCs showed high intensity of the QD_{612} emission (Fig. 2*A*, *Center*). We then tested whether $QD_{612}^{NB\text{-}Tz}$Ab(CD45) labeled all $CD45^+$ cells by incubating PBMNCs with $QD_{612}^{NB\text{-}Tz}$Ab(CD45) and Ab(CD45)-PE/Cy7 (commercial Ab) simultaneously. Fig. 2*A*, *Right* shows a good correlation between the signals from Ab(CD45)-PE/Cy7 and $QD_{612}^{NB\text{-}Tz}$Ab (CD45), confirming efficient and specific immunostaining. The specificity of $QD_{612}^{NB\text{-}Tz}$Ab(Sca-1) and $QD_{570}^{NB\text{-}Tz}$Ab(c-Kit), which are used for single-cell imaging in vivo, was also tested similarly with viable BMCs that were extracted from tibia and femur bones of FVB mice. As expected, a good correlation between the signal from $QD^{NB\text{-}Tz}$Ab and commercial antibodies was observed (Fig. 2*B*). Of note, the expression level of antigens varies significantly depending on both the type of antigen and the cell type. Therefore, in some cases, antigen-positive cells are clearly distinguishable from antigen-negative cells (Fig. 2*A*), whereas in the other cases, the antigen expression level is rather continuous (Fig. 2*B*).

In Vivo Specificity Study and Optimization of the Ratio Between QDs and Abs

Before proceeding to single-cell labeling, we tested the in vivo specificity of our QD-Ab conjugates by labeling blood vessels, which are mesoscale objects. For the in vivo specificity test, QDs or QD-Ab conjugates were administered through systemic injection in the retro-orbital sinus to ^{Tie2}GFP/FVB transgenic mice, which selectively express GFPs in endothelial cells, and the blood vessels were imaged through a mammary fat pad window using a multiphoton microscope. Nonspecific binding of QD^{NB} and $QD^{NB\text{-}Tz}$Ab to cells and tissue was first tested by injecting QD_{612}^{NB} and $QD_{612}^{NB\text{-}Tz}$Ab(IgG) and imaging vessels over 24 h. Fig. 3 *A* and *B* and *SI Appendix*, Fig. S11 show that both of QD_{612}^{NB} and $QD_{612}^{NB\text{-}Tz}$Ab(IgG) were cleared from the blood circulation within 20 h with no evidence of nonspecific accumulation. In contrast, we observed nonspecific accumulation of commercial Qdot 625 and Qdot 625-Ab(IgG) in random spots after the QDs were cleared from systemic circulation (Fig. 3 *C* and *D* and *SI Appendix*, Fig. S12). In vivo specificity of $QD^{NB\text{-}Tz}$Ab was then studied by injecting $QD^{NB\text{-}Tz}$Ab(CD31) systemically and monitoring the labeling signals of endothelial cells over time. Colocalization of the QD signal with the GFP signal confirmed the specificity of the $QD_{612}^{NB\text{-}Tz}$Ab(CD31) toward endothelial cells (Fig. 3 *E* and *F*).

The performance of $QD^{NB\text{-}Tz}$Ab samples with different ratios between QDs and Abs was evaluated to achieve bright and stable labeling signal in the vessel-labeling study. QD-Ab conjugates containing a higher number of QDs are expected to yield a brighter signal; however, a high number of QDs per Ab may increase the chance of detachment of $QD^{NB\text{-}Tz}$Ab from the labeled objects by perturbing the binding kinetics (lower affinity) or triggering unexpected effects in vivo. To find the best ratio, we synthesized $QD^{NB\text{-}Tz}$Ab(CD31) with QD to Ab(CD31) ratios of 3:1, 1:1, and 1:3 and analyzed the intensity and pattern of the labeling signals. As shown in Fig. 3 *E* and *F* and *SI Appendix*, Fig. S13, $QD_{612}^{NB\text{-}Tz}$Ab(CD31) with all three ratios specifically labeled the GFP^+ vascular endothelium from 3 to 4 h up to 24 h after systemic injection. After 24 h, the QD signal from the vessels was still visible, but the observed pattern became more punctate. The punctate staining pattern may be caused by either endocytosis of the $QD_{612}^{NB\text{-}Tz}$Ab(CD31) into endothelial cells or detachment of the probe because of low affinity. The analyses of the labeling intensities of vessels illustrate that the signal was greater for $QD^{NB\text{-}Tz}$Ab(CD31) having a higher ratio of QDs but that the punctate pattern was also more dominant (*SI Appendix*, Figs. S14 and S15). To achieve a balance between signal intensity and signal stability, we chose the $QD^{NB\text{-}Tz}$Ab with the QD:Ab ratio of 1:1 for in vivo cytometry experiments.

Multiplexed Single-Cell Imaging in Vivo

We used our newly developed $QD^{NB\text{-}Tz}$Ab to show the imaging of single cells from an endogenous rare population in unmanipulated mice. As an example of rare cells, $Sca1^+c\text{-}Kit^+$ cells in the intact calvarial bone were imaged through a newly established chronic calvarial window placed in C57/BL6 mice. In mice, $Sca1^+c\text{-}Kit^+$ cells consist of multipotent progenitors (short- and long-term hematopoietic stem cells) (21), which generate all blood cells throughout the lifetime of the organism. Although the function of hematopoietic stem and progenitor cells has been well-characterized, locating the cell niche within the entire bone marrow and studying cellular dynamics in their native

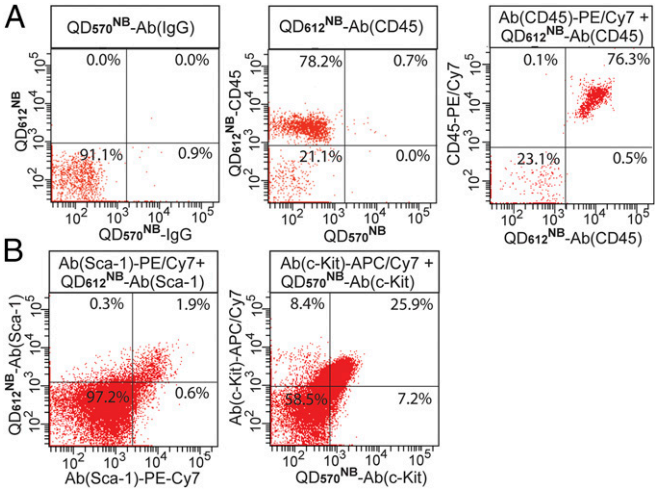

Fig. 2. In vitro specificity of $QD^{NB\text{-}Tz}$Ab nanoconjugates. (*A*) Flow cytometric analysis of PBMNCs immune-stained with QD nanoconjugates. Fluorophore signal intensities for each cell, represented with red dots, are plotted on two axes. (*Left*) Nonspecific binding test of $QD_{570}^{NB\text{-}Tz}$Ab(IgG) to PBMNCs shows that $QD_{570}^{NB\text{-}Tz}$Ab(IgG) displays minimal nonspecific binding to cells. (*Center*) After incubation of PBMNCs with $QD_{612}^{NB\text{-}Tz}$Ab(CD45), >75% of PBMNCs were labeled with $QD_{612}^{NB\text{-}Tz}$Ab(CD45). (*Right*) After incubating PBMNCs with $QD_{612}^{NB\text{-}Tz}$Ab(CD45) and Ab(CD45)-PE/Cy7, strong correlation was observed between the signals from $QD_{612}^{NB\text{-}Tz}$Ab(CD45) and Ab(CD45)-PE/Cy7. This result proves specificity of the $QD^{NB\text{-}Tz}$Ab(CD45). (*B*) Flow cytometric analysis of BMCs. Incubation of $Lineage^-$ BMCs with (*Left*) $QD_{612}^{NB\text{-}Tz}$Ab(Sca-1) and the Ab(Sca-1)-PE/Cy7 and (*Right*) $QD_{570}^{NB\text{-}Tz}$Ab(c-Kit) and the Ab(c-Kit)-APC/Cy7. Strong correlation between the signals from (*Left*) $QD_{612}^{NB\text{-}Tz}$Ab(Sca-1) and Ab(Sca-1)-PE/Cy7 and (*Right*) $QD_{570}^{NB\text{-}Tz}$Ab(c-Kit) and Ab(c-Kit)-APC/Cy7 proves the specificity of the $QD^{NB\text{-}Tz}$Ab(Sca-1) and $QD^{NB\text{-}Tz}$Ab(c-Kit).

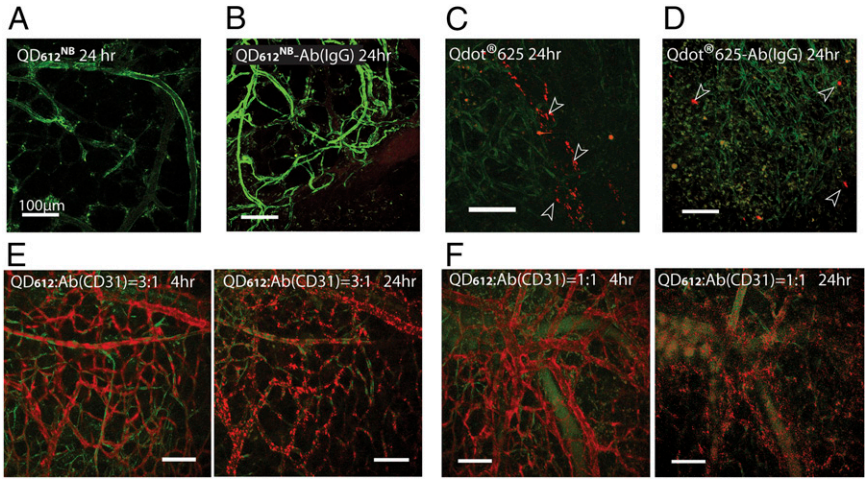

Fig. 3. In vivo microscopy imaging of blood vascular endothelial cells using QD-Ab conjugates. (*A*–*D*) Imaging of nonspecific binding for (*A*) QD_{612}^{NB}, (*B*) $QD_{612}^{NB\text{-}Tz}$Ab(IgG), (*C*) Qdot 625 (commercial), and (*D*) Qdot625-Ab(IgG) (commercial). QD_{612}^{NB} and $QD_{612}^{NB\text{-}Tz}$Ab(IgG) display virtually no nonspecific binding, whereas commercial Qdot 625 and Qdot625-Ab (IgG) show significant nonspecific binding. (*E* and *F*) Labeling of endothelial cells using the $QD_{612}^{NB\text{-}Tz}$Ab (CD31). Images taken at 4 and 24 h after the injection of $QD_{612}^{NB\text{-}Tz}$Ab(CD31) synthesized at QD:Ab ratios of (*E*) 3:1 and (*F*) 1:1 show that $QD_{612}^{NB\text{-}Tz}$Ab(CD31) with different ratios specifically labeled the GFP^+ vascular endothelium from 3 to 4 h up to 24 h after systemic injection. Green and red signals represent fluorescence from GFP^+ vascular endothelium and QDs, respectively.

environments have been challenging because of the lack of appropriate methodologies (22). Recently, a method combining laser-scanning cytometry on tissue sections and confocal/multiphoton microscopy on thick femoral bone marrow slices was reported to study distribution patterns and the oxygenation status of stem cell niches in the entire femoral bone marrow (23). However, even this method used bone sectioning followed by ex vivo imaging. Our single cell-labeling method enables single $Sca1^+c\text{-}Kit^+$ cell imaging across the entire calvarial window in unmanipulated live animals.

Intactness of a newly developed calvarial window was tested by performing single-photon imaging of the bone marrow of ^{Actb}GFP/C57BL/6 mice, which express GFP ubiquitously in all cells. As shown in *SI Appendix*, Fig. S18, the bone marrow can be imaged from day 0 to day 8 without any signs of inflammation or hemorrhage.

Unbiased statistical analyses from single-cell imaging requires fluorescent probes that diffuse into the entire area of interest and label all of the cells of interest. To verify whether $QD^{NB\text{-}Tz}$Ab diffuses throughout the whole bone marrow, we injected $QD^{NB\text{-}Tz}$Ab (CD45) into FVB mice through the tail vein, and we analyzed the percentage of $CD45^+$ BMCs that are labeled with our QD immunoconstructs. The diffusion of our newly developed $QD^{NB\text{-}Tz}$Ab in vivo was then compared with that of commercially available antibodies. The diffusion experiment was carried out by (*i*) administering $QD^{NB\text{-}Tz}$Ab(CD45) or commercial Ab (CD45)-APC through the tail vein into mice, (*ii*) waiting 24 h to allow the Ab-based probes to clear from vessels and interstitial space, (*iii*) extracting BMCs from tibia and femur bones, (*iv*) staining BMCs with Ab(CD45)-PE/Cy7 ex vivo, and (*v*) analyzing the proportion of $CD45^+$ BMCs that are labeled with $QD^{NB\text{-}Tz}$Ab (CD45) using flow cytometry (Fig. 4*A*). To target cells in vivo, the Ab probes used in step *i* need to extravasate from vessels and diffuse throughout the interstitial space. In contrast, Ab(CD45)-PE/Cy7 used in step *iv* is directly incubated with BMCs and therefore, labels all $CD45^+$ BMCs. Fig. 4 *B* and *C* shows the flow cytometry results on entire BMCs that have gone through the procedures described above. The horizontal axis in Fig. 4 *B* and *C* is the fluorescent intensity from $QD_{612}^{NB\text{-}Tz}$Ab(CD45), and the vertical axis in Fig. 4 *B* and *C* is the fluorescent intensity from Ab (CD45)-PE/Cy7. $CD45^+$ BMCs are colored green [based on the Ab(CD45)-PE/Cy7 signal] and $CD45^-$ BMCs are colored red in Fig. 4 *B* and *C*. As shown in Fig. 4 *B* and *C*, there were almost no nonspecifically labeled cells, which would be Ab(CD45)-PE/Cy7–negative and $QD_{612}^{NB\text{-}Tz}$Ab(CD45)– or Ab(CD45)-allophycocyanin (APC)–positive. In in Fig. 4 *B*, *Right* and *C*, *Right*, both $CD45^+$ BMCs (green) and $CD45^-$ BMCs (red) are replotted against the signal of the probes injected in vivo to clearly compare the diffusion of $QD_{612}^{NB\text{-}Tz}$Ab(CD45) (Fig. 4*B*) and Ab(CD45)-APC (Fig. 4*C*). In Fig. 4*B*, most $CD45^+$ BMCs (green) displayed high fluorescent intensity in the $QD_{612}^{NB\text{-}Tz}$Ab(CD45) channel, which indicates that $QD_{612}^{NB\text{-}Tz}$Ab(CD45) successfully labeled most of $CD45^+$ BMCs. In comparison, a bimodal distribution (stained and nonstained) of the Ab(CD45)-APC signal intensities was observed for $CD45^+$ BMCs in Fig. 4*C*. This bimodal distribution indicates that Ab(CD45)-APC did not label >30% of $CD45^+$ BMCs (Fig. 4*C*). Considering that the same amount of Ab was injected in both experiments (100 μg), we can conclude that $QD_{612}^{NB\text{-}Tz}$Ab(CD45) is more efficient in labeling $CD45^+$ BMCs than Ab(CD45)-APC. The higher population of observed labeled cells using QD immunoconstructs than using commercial antibodies may be explained by the higher optical absorption coefficient of QDs. Because of their high absorption coefficient, we expect that fewer QD conjugates are required for visualizing single cells in vivo than commercial antibodies. Based on our diffusion study, we claim that it is easier to detect cells that are distant from vessels using our QD conjugates than commercial antibodies. Differences in the deep tissue-labeling performance between the QD conjugates and the dye-labeled antibodies are even more extreme for multiphoton microscopy, because the multiphoton action cross-section is at least two orders of magnitude lower for organic dyes than for QDs (24).

Labeling of single cells from rare populations of hematopoietic stem and progenitor cells was successfully achieved using our QD immunoconstructs and multiphoton microscopy. Multiphoton microscopy was used to increase the imaging depth and minimize cell damage and background signals. As imaging probes, $QD_{570}^{NB\text{-}Tz}$Ab(c-Kit) and $QD_{612}^{NB\text{-}Tz}$Ab(Sca-1) (popular cell markers for hematopoietic stem and progenitor cells), $QD_{800}^{NB\text{-}Tz}$Ab(IgG) (nonspecific control), and Hoechst 33342 (a DNA-binding dye that labels most of the cells in the bone marrow) were injected retro-orbitally in mice. Contrast-enhanced angiography was used to detect the bone marrow vessels, and second harmonic generation microscopy was used to image the bone (3) (Fig. 5). Intravital multiphoton microscopy imaging was performed 24 h after the injection of the $QD^{NB\text{-}Tz}$Ab when unbound $QD^{NB\text{-}Tz}$Ab was completely cleared from the blood circulation and the bone marrow interstitial space (25). Twenty-four hours after the injection, we observed that ∼0.3% of cells within the bone marrow were labeled with $QD^{NB\text{-}Tz}$Ab(Sca-1) and $QD^{NB\text{-}Tz}$Ab(c-Kit), but none were labeled with $QD_{800}^{NB\text{-}Tz}$Ab(IgG) (Fig. 5 and *SI Appendix*, Figs. S19–S21). To confirm that we labeled all $Sca1^+c\text{-}Kit^+$ cells from BMCs, we extracted BMCs from tibia and femur bones, stained them with Ab(Sca-1)-PE/Cy7 and Ab(c-Kit)-APC/Cy7 ex vivo, and analyzed

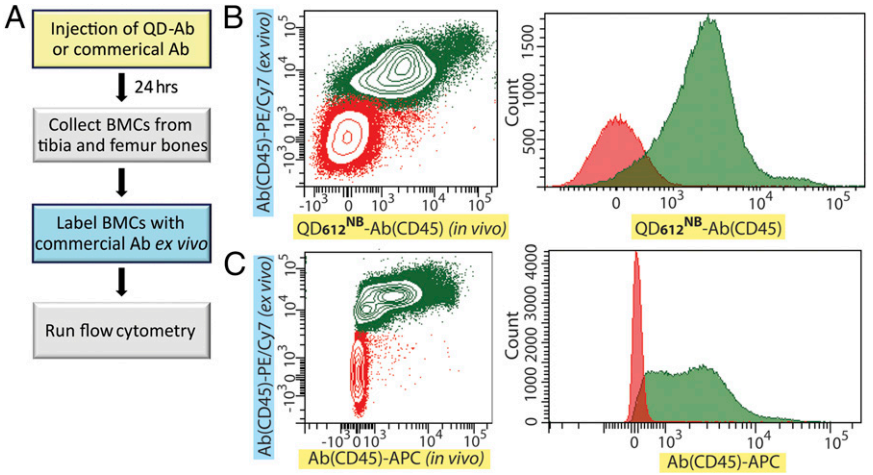

Fig. 4. Analysis on in vivo diffusion of QD conjugates in bone marrow. (*A*) Experimental scheme. *B*, *Left* and *C*, *Left* are 2D plots of BMCs against the in vivo-stained probe signal (*x* axis; yellow box in *A*) and ex vivo-stained probe signal (*y* axis; blue box in *A*). $CD45^+$ BMCs (green) were clearly distinguished from $CD45^-$ BMCs (red) based on the Ab(CD45)-APC signal. In *B*, *Right* and *C*, *Right*, both $CD45^+$ BMCs (green) and $CD45^-$ BMCs (red) are replotted against the in vivo-stained probe to clearly compare the diffusion of (*B*) QD_{612}^{NB}-Ab(CD45) with the diffusion of (*C*) Ab(CD45)-APC. (*B*) Most of the $CD45^+$ BMCs (green) were stained with $QD_{612}^{NB\text{-}Tz}$Ab (CD45). (*C*) Bimodal distribution of the Ab(CD45)-APC signal intensities (stained and nonstained) was observed for $CD45^+$ BMCs, which indicates that Ab(CD45)-APC did not label entire $CD45^+$ BMCs.

the percentage of $Sca1^+$, c-Kit^+, and $Sca1^+$c-Kit^+ cells using flow cytometry. As shown in *SI Appendix*, Fig. S22, populations of c-Kit^+, $Sca1^+$, and $Sca1^+$c-Kit^+ cells were 2.779%, 2.132%, and 0.217%, respectively. The numbers closely match with the percentages that are labeled with $QD^{NB\text{-}Tz}$Ab(c-Kit), $QD^{NB\text{-}Tz}$Ab(Sca-1), and $QD^{NB\text{-}Tz}$Ab(Sca-1)/$QD^{NB\text{-}Tz}$Ab(c-Kit) in vivo, which were ~3%, ~1.7%, and ~0.3%, respectively. The consistency between in vitro and in vivo studies shows that our QD-Ab conjugates specifically and accurately label cells in vivo. Note that these population percentages are calculated from entire BMCs and not from $Lineage^-$ BMCs. A detailed method for processing raw images and identifying $Sca1^+$c-Kit^+ cells is described in *SI Appendix*, Fig. 19. In addition, we were able to track single cells in calvarial bone marrow for an extended period (>3 h). Movie S1 shows a stably bound intravascular $Sca1^+$c-Kit^+ cell interacting with a rolling WBC.

Lastly, we proved that the color or the composition of the QDs does not affect the quality of the imaging by labeling $Sca1^+$c-Kit^+ cells using $QD^{NB\text{-}Tz}$Ab with different combinations of QDs and antibodies [$QD_{800}^{NB\text{-}Tz}$Ab(c-Kit) and $QD_{612}^{NB\text{-}Tz}$Ab(Sca-1)]. In this experiment, bone marrow vessels were visualized using endogenous GFP expression in endothelial cells in transgenic ^{Tie2}GFP/FVB mice. *SI Appendix*, Fig. S23 shows successful labeling of $Tie2^+$ $Sca1^+$c-Kit^+ and $Tie2^-Sca1^+$c-Kit^+ cells, which shows that diverse combinations of $QD^{NB\text{-}Tz}$Abs that emit from the visible to the near-IR (NIR) can be used for multiplexed phenotypic imaging in vivo.

Conclusions

For single endogenous cell labeling for microscopy imaging in animals, fluorescent probes are administered systemically and delivered to the target site through extravasation and diffusion. Because the delivery determines the effective concentration of the probes available for cell targeting, fluorophores for single-cell tracking should meet highly strict criteria, such as compact size, neutral charge, high brightness, high purity, and extremely low

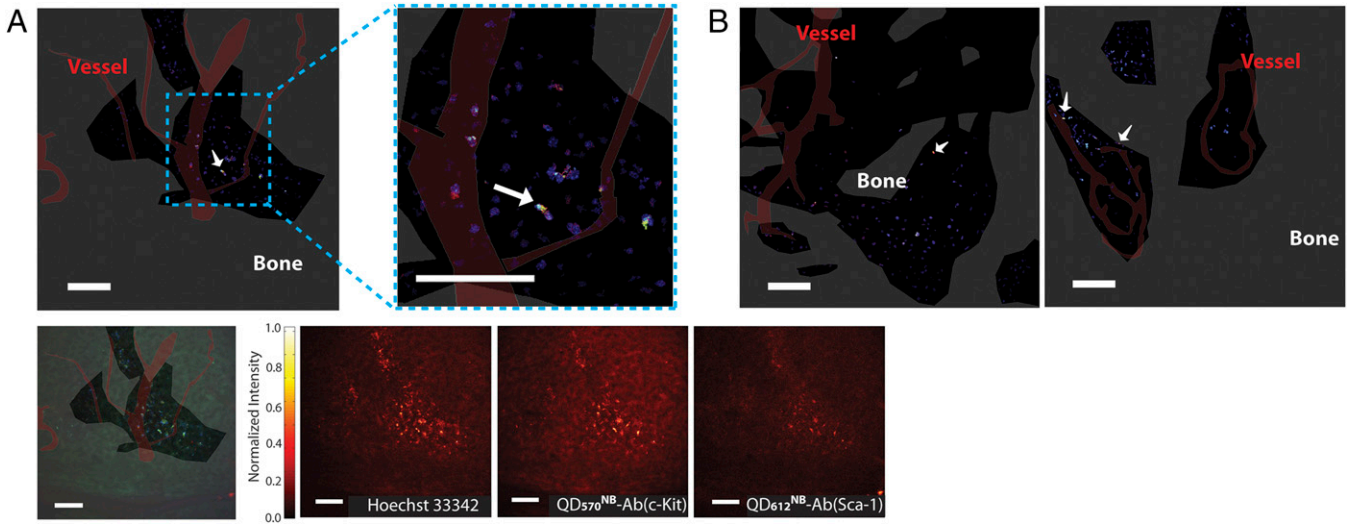

Fig. 5. In vivo imaging of single endogenous Sca-1^+c-Kit^+ cells in the intact bone marrow using $QD^{NB\text{-}Tz}$Ab. (*A*, *Upper*) A representative multiphoton microscopy image of a bone marrow cavity shown after removing the signal from the QD/Ab channels outside of the cells, which were segmented from Hoechst 33342 signal. Yellow cells (arrows) represent single Sca-1^+c-Kit^+ cells. Red and green cells represent Sca-1^+ and c-Kit^+ cells, respectively. An area containing an Sca-1^+c-Kit^+ cell is magnified in *Upper Right*. Translucent red and gray areas represent vessels and the bone, respectively. *Lower Left* shows the unmodified maximum intensity projection (~10 μm in the *z* direction). *Lower Right* shows the maximum intensity projections of each channel individually. (*B*) Additional images of bone marrow cavities containing Sca-1^+c-Kit^+ cells. Signals outside of the Hoechst 33342^+ cells were discarded in these images, e.g., in *A*, *Upper*. (Scale bars: 100 μm.)

nonspecific interactions with biomolecules. These design rules are much more stringent than those for commonly used in vitro probes, where the probes are delivered to target cells by direct incubation. For in vitro labeling, the lack of nonspecific binding to serum/cell and the high purity of the probes are less critical owing to intense signals from the high concentration of labeling probes. The size of the probes is also not as critical as it is for in vivo labeling, where diffusion in the dense in vivo environment must be efficient to reach target cells.

Because of the strict requirements for single cell-labeling probes in vivo, the development of such fluorophores requires innovation and rigorous characterization. Here, we present QD-Ab conjugates that (*i*) are easily and efficiently derivable with targeting molecules or secondary reporters, (*ii*) display high stability and maintain a high QY in complex in vivo environments, (*iii*) possess minimal nonspecific cell/serum binding, (*iv*) exhibit long circulation half-life for enhanced delivery to target sites, (*v*) are purified thoroughly from unbound targeting molecules, because free-targeting molecules can block target sites and yield a significantly decreased QD signal, (*vi*) have a compact size for enhanced diffusion throughout dense in vivo environments, and (*vii*) have narrow emission for multiplexed imaging. $QD^{NB\text{-}Tz}$Ab conjugates bind specifically to cellular antigens both in vitro and in vivo and perform better than the commercial antibodies that we tested to label BMCs after systemic injection. Our in vivo microscopy imaging results show the applicability of QD-Ab conjugates for multiplexed in vivo cytrometric imaging of endogenous rare cells in unmanipulated mice. Note that the QD probes have several advantages over fluorescently labeled commercial Abs. Commercial fluorescent Abs use organic dyes (e.g., Phycobilins and Cy7) as chromophores, and there are many disadvantages associated with organic dyes, such as small multiphoton action cross-section, low photostability under intense illumination, and asymmetric emission with red tails.

This technique offers new possibilities to study single-cell interactions and responses and their microenvironments in live animals. First, intense and stable fluorescent signal of QDs allows long-term tracking of single cells in intact or diseased tissues in vivo. Second, our technique can be applied to unmanipulated animals as opposed to genetically modified, immunodeficient, or preirradiated mice. This method may be useful for the functional analysis of single endogenous cells in their native environments, such as measuring the oxygen level, glucose concentration, or local mechanical stress near the cell of interest. Oxygen measurements in the bone marrow and the Ska-1^{+}c-Kit^{+} cell niche will be presented elsewhere. Third, the high photostability of QDs allows for FRET studies in vivo for extended periods, which can be used to study the microenvironments of target cells and cellular interactions. High photostability is essential for FRET studies to maintain the QY of donors and acceptors constant. Fourth, the technique described here can be extended to single-cell imaging in deep tissues or highly scattering environments by the use of NIR/IR QD-Ab conjugates. QDs are especially useful for NIR/IR imaging, because NIR/IR dyes display limited QY and orders of magnitude lower photostability (26, 27). The challenges addressed and overcome in this paper are not limited to QDs. Our work provides insights for the rational design of any nanoconstructs for in vivo applications.

Materials and Methods

Detailed methods on the following subjects are available in *SI Appendix, SI Materials and Methods*: vendor information on the antibodies, mice models, synthesis of QDs, QD ligands, tetrazine-modified Abs and $QD^{NB\text{-}Tz}$Ab conjugates, fluorescence correlation spectroscopy, purification of $QD^{NB\text{-}Tz}$Ab using gradient centrifugation, bicinchoninic acid (BCA) assay for the measurement of the ratios of QD to Ab in the $QD^{NB\text{-}Tz}$Ab conjugates, flow cytometry (including gating and compensation strategies), preparation of chronic bone marrow window, intravital multiphoton imaging, physiological monitoring of mice during intravital microscopy, and image analysis.

ACKNOWLEDGMENTS. This research is supported by National Institute of Health Grants R01-CA126642, R01-CA115767, and P01-CA080124 (to R.K.J.), R01-CA096915 (to D.F.), U54-CA151884 and P41-EB015871-26A1 (to M.G.B.), R21-CA139168 (to D.G.D.), and R01-CA159258 (to D.G.D.); Department of Defense Breast Cancer Research Innovator Award W81XWH-10-1-0016 (to R.K.J.); American Cancer Society Grant RSG-11-073-01-346TBG (to D.G.D.); a postdoctoral fellowship from the Susan G. Komen Foundation (to W.S.K.); a graduate student fellowship from the Samsung Scholarship (to H.-S.H.); Massachusetts Institutes of Technology Department of Chemistry Instrumentation Facility Grants CHE-980806 and DBI-9729592; Institute for Soldier Nanotechnology Grant W911NF-07-D-0004 (to M.G.B.); and National Science Foundation-Materials Research Science and Engineering Centers Program DMR-0117795 through the use of its shared user facilities.

1. Kiel MJ, et al. (2005) SLAM family receptors distinguish hematopoietic stem and progenitor cells and reveal endothelial niches for stem cells. *Cell* 121(7):1109–1121.
2. Xie Y, et al. (2009) Detection of functional haematopoietic stem cell niche using real-time imaging. *Nature* 457(7225):97–101.
3. Lo Celso C, et al. (2009) Live-animal tracking of individual haematopoietic stem/progenitor cells in their niche. *Nature* 457(7225):92–96.
4. Livet J, et al. (2007) Transgenic strategies for combinatorial expression of fluorescent proteins in the nervous system. *Nature* 450(7166):56–62.
5. Kedrin D, et al. (2008) Intravital imaging of metastatic behavior through a mammary imaging window. *Nat Methods* 5(12):1019–1021.
6. Swirski FK, et al. (2009) Identification of splenic reservoir monocytes and their deployment to inflammatory sites. *Science* 325(5940):612–616.
7. Dabbousi BO, et al. (1997) (CdSe)ZnS core-shell quantum dots: Synthesis and characterization of a size series of highly luminescent nanocrystallites. *J Phys Chem B* 101(46):9463–9475.
8. Bruchez M, Jr, Moronne M, Gin P, Weiss S, Alivisatos AP (1998) Semiconductor nanocrystals as fluorescent biological labels. *Science* 281(5385):2013–2016.
9. Peng ZA, Peng X (2001) Formation of high-quality CdTe, CdSe, and CdS nanocrystals using CdO as precursor. *J Am Chem Soc* 123(1):183–184.
10. Zimmer JP, et al. (2006) Size series of small indium arsenide-zinc selenide core-shell nanocrystals and their application to in vivo imaging. *J Am Chem Soc* 128(8): 2526–2527.
11. Gao X, Cui Y, Levenson RM, Chung LWK, Nie S (2004) In vivo cancer targeting and imaging with semiconductor quantum dots. *Nat Biotechnol* 22(8):969–976.
12. Popović Z, et al. (2010) A nanoparticle size series for in vivo fluorescence imaging. *Angew Chem Int Ed Engl* 49(46):8649–8652.
13. Wong C, et al. (2011) Multistage nanoparticle delivery system for deep penetration into tumor tissue. *Proc Natl Acad Sci USA* 108(6):2426–2431.
14. So M-K, Xu C, Loening AM, Gambhir SS, Rao J (2006) Self-illuminating quantum dot conjugates for in vivo imaging. *Nat Biotechnol* 24(3):339–343.
15. Stroh M, et al. (2005) Quantum dots spectrally distinguish multiple species within the tumor milieu in vivo. *Nat Med* 11(6):678–682.
16. Han H-S, et al. (2010) Development of a bioorthogonal and highly efficient conjugation method for quantum dots using tetrazine-norbornene cycloaddition. *J Am Chem Soc* 132(23):7838–7839.
17. Liu W, et al. (2010) Compact biocompatible quantum dots via RAFT-mediated synthesis of imidazole-based random copolymer ligand. *J Am Chem Soc* 132(2):472–483.
18. Choi HS, et al. (2007) Renal clearance of quantum dots. *Nat Biotechnol* 25(10): 1165–1170.
19. Howarth M, et al. (2008) Monovalent, reduced-size quantum dots for imaging receptors on living cells. *Nat Methods* 5(5):397–399.
20. Xiao K, et al. (2011) The effect of surface charge on in vivo biodistribution of PEG-oligocholic acid based micellar nanoparticles. *Biomaterials* 32(13):3435–3446.
21. Yang L, et al. (2005) Identification of Lin(-)Sca1(+)kit(+)CD34(+)Flt3- short-term hematopoietic stem cells capable of rapidly reconstituting and rescuing myeloablated transplant recipients. *Blood* 105(7):2717–2723.
22. Kiel MJ, Morrison SJ (2008) Uncertainty in the niches that maintain haematopoietic stem cells. *Nat Rev Immunol* 8(4):290–301.
23. Nombela-Arrieta C, et al. (2013) Quantitative imaging of haematopoietic stem and progenitor cell localization and hypoxic status in the bone marrow microenvironment. *Nat Cell Biol* 15(5):533–543.
24. Larson DR, et al. (2003) Water-soluble quantum dots for multiphoton fluorescence imaging in vivo. *Science* 300(5624):1434–1436.
25. Brown EB, et al. (2001) In vivo measurement of gene expression, angiogenesis and physiological function in tumors using multiphoton laser scanning microscopy. *Nat Med* 7(7):864–868.
26. Resch-Genger U, Grabolle M, Cavaliere-Jaricot S, Nitschke R, Nann T (2008) Quantum dots versus organic dyes as fluorescent labels. *Nat Methods* 5(9):763–775.
27. Kim S, et al. (2004) Near-infrared fluorescent type II quantum dots for sentinel lymph node mapping. *Nat Biotechnol* 22(1):93–97.